

Deep Near Infrared Imaging toward Vela Molecular Ridge C - 1: A Remarkable Embedded Cluster in RCW 36 -

D. Baba^{1,2}, T. Nagata¹, T. Nagayama¹, C. Nagashima¹, D. Kato¹, M. Kurita¹, S. Sato¹,
Y. Nakajima³, M. Tamura³, H. Nakaya⁴, and K. Sugitani⁵

ABSTRACT

We present deep near-infrared (J, H, K_S) images toward an embedded cluster which lies in a $C^{18}O$ clump in the cloud C of the Vela Molecular Ridge. This cluster has at least ~ 350 members and a radius of ~ 0.5 pc. The stellar surface number density is approximately 3000 stars pc^{-2} in the central $0.1 \text{ pc} \times 0.1 \text{ pc}$ region of the cluster. This is much higher than most of the young clusters within 1 kpc of the Sun. From the comparison of the luminosity function and near-infrared excess fraction with those of other embedded clusters, we estimate that the age of this cluster is approximately 2-3 Myr. This cluster exhibits an excess of brighter stars in its central region, from which we conclude that the more massive stars are located near the cluster center.

Subject headings: ISM: clouds — ISM: individual (Vela Molecular Ridge) — stars: formation — stars: luminosity function, mass function

1. INTRODUCTION

The progress of NIR array detectors provided opportunities to observe stellar contents in molecular clouds. Many studies of these regions revealed the presence of stellar clusters which are deeply embedded in molecular clouds (Lada et al. 1991; Carpenter et al. 1993;

¹Department of Physics, Nagoya University, Chikusa-ku, Nagoya 464-8602, Japan

²e-mail: baba@z.phys.nagoya-u.ac.jp

³National Astronomical Observatory of Japan, Mitaka, Tokyo 181-8588, Japan

⁴Subaru Telescope, National Astronomical Observatory of Japan, Hilo, HI 96720

⁵Institute of Natural Sciences, Nagoya City University, Mizuho-ku, Nagoya 467-8501, Japan

Hodapp 1994). Statistical studies revealed that the most of young stellar objects in giant molecular clouds (GMCs) are formed in embedded clusters (Lada & Lada 2003). These embedded clusters are typically found to have their most massive stars in the central region (the position whose stellar densities are the highest) (Zinnecker, McCaughrean, & Wilking 1993; Hillenbrand & Hartmann 1998). Several embedded clusters also shows mass segregation; more massive stars tend to be located in the central region [e.g., Trapezium (Hillenbrand & Hartmann 1998); NGC 2024, NGC 2071 (Lada et al. 1991); NGC 3603 (Nürnberg & Petr-Gotzens 2002)]. However, Carpenter et al. (1997) pointed out that there is no evidence of mass segregation in the Mon R2 cluster. Unfortunately, the mass segregation has been investigated only for a few embedded clusters. We need more samples for statistical studies.

In this paper, we study an embedded cluster which lies in a C¹⁸O clump identified by Yamaguchi et al. (1999) in the cloud C of the Vela Molecular Ridge (VMR). The VMR is a GMC complex, being composed of at least four GMCs (named A, B, C, and D) with individual masses exceeding $10^5 M_{\odot}$ (Murphy & May 1991). The clouds A, C, and D are located at 700 ± 200 pc, and the cloud B is located at ~ 2 kpc (Liseu et al. 1992). The cloud C is the richest in molecular gas and the least evolved of the complex (Yamaguchi et al. 1999). This embedded cluster was recently discovered by Massi, Lorenzetti, & Giannini (2003) in their NIR imaging survey toward Class I sources in VMR (Liseu et al. 1992; Lorenzetti, Spinoglio, & Liseu 1993). Massi, et al. (2003) found that high mass stars which excite the H II region RCW 36 lie in this cluster (hereafter RCW 36 cluster). However, due to the relatively small image dimensions, their observations were not able to cover the whole cluster. Therefore, the fundamental properties of the RCW 36 cluster, such as the number of the stars, radius and the stellar distribution, have been still unknown. Our observation first provides the detailed census of the RCW 36 cluster.

2. OBSERVATIONS AND DATA REDUCTION

The NIR images of RCW 36 were obtained on 2002 March 9 with the NIR camera SIRIUS (Simultaneous three-color InfraRed Imager for Unbiased Survey) mounted on the IRSF (InfraRed Survey Facility) 1.4 m telescope of Nagoya University at Sutherland, South African Astronomical Observatory. SIRIUS is equipped with three 1024×1024 pixel HgCdTe arrays. Dichroic mirrors enable simultaneous observations in the J , H , and K_S bands (Nagashima et al. 1999; Nagayama et al. 2002). The image scale of the array is $0''.45 \text{ pixel}^{-1}$, giving a field of view of $7'.7 \times 7'.7$. Ten dithered frames were observed as a set of exposures. We observed three sets of the object and sky frames alternatively with a 30 second exposure. We also observed one set of the object and sky frames with a 5 second exposure for bright sources.

Seeing condition was $\sim 1''.1$ (FWHM) in the K_S band. We observed the standard star 9136 in the faint near-infrared standard star catalog of Persson et al. (1998) for photometric calibration.

We applied the standard procedures of near-infrared array image reduction, including dark current subtraction, sky subtraction, and flat-fielding, using the IRAF (Imaging Reduction and Analysis Facility) ¹ software package. Identification and photometry of point sources were performed by using the DAOPHOT packages in IRAF. In order to avoid the affection for the photometry from the nearby stars, we used a radius of ~ 3 pixels ($1''.35$) in the PSF fitting in the DAOPHOT task.

The limiting magnitudes (at 10σ) are estimated to be ~ 19.0 , 18.0 , and 16.6 in the J , H , and K_S bands, respectively. A total number of 823 sources are detected in the K_S band with a photometric error of ≤ 0.1 mag, and 610 sources are identified in the three bands with a photometric error of ≤ 0.1 mag and with a positional agreement of $\leq 0.5''$. In order to determine the completeness limit of the photometry, we added artificial stars to the central region of the image (dotted square in Fig. 2) with $17''$ spacing. We define the magnitudes at which 90% of stars were detected as the completeness limits. They are 18.2 , 16.9 , and 16.3 at J , H , and K_S , respectively.

3. RESULTS

3.1. NIR image

In Fig. 1, we show a composite JHK_S color image of the RCW 36 cluster. It clearly shows that the stars concentrate at the center of the image. The brightest star located at $8^h59^m27^s.5$, $-43^\circ45'27''$ (J2000) is the exciting star (O8 or two O9 stars; Verma et al. 1994) of RCW 36 (Massi, et al. 2003). At optical wavelengths, the stellar cluster including the exciting star is hidden by a dark-lane across RCW 36. The radio continuum peak position is $\sim 35''$ west of the exciting star (shown by plus in Fig. 1; Walsh et al. 1998); this coincide spatially with a bright nebula. An H_2O maser is detected $\sim 30''$ west of the exciting star (shown by asterisk in Fig. 1; Braz & Epchtein 1982); there is no NIR counterpart. The existence of the H_2O maser means that star formation is still ongoing in the RCW 36 cluster. There are several bright-rimmed clouds at $\sim 1'$ west, $\sim 1'$ south, and $\sim 2'$ south-east of the

¹IRAF is distributed by the National Optical Astronomy Observatories, which are operated by the Association of Universities for Research in Astronomy, Inc., under cooperative agreement with the National Science.

exciting star. They are likely to be dense cores which were revealed by evaporation of a molecular cloud due to UV photons from the exciting star.

3.2. Stellar Census in the RCW 36 Cluster

3.2.1. Stellar Surface Number Density

In Fig. 2, we show the contour map of the stellar surface number density (SSND) derived from 823 sources detected at K_S with a photometric error of ≤ 0.1 mag. The SSND is obtained by counting stars in a $30'' \times 30''$ area every $15''$ over the K_S image. At the distance of 700 pc, the unit cell of $30'' \times 30''$ corresponds to ~ 0.1 pc \times 0.1 pc. The frequency distribution of the star counts (in stars per unit cell) can be fitted by the Poisson function with a mean of 2.0 stars per unit cell, plus the wing where excess of counts due to the central clustering appear. The SSND shows two peaks. The northern peak coincides spatially with the exciting star and shows the highest SSND. The southern one coincides spatially with one of the bright rims at $\sim 1'$ south of the exciting star.

3.2.2. Radial Profile

In Fig. 3, we show the radial profile of the SSND for the RCW 36 cluster. The SSND is measured in circular annuli, centering on the location of the peak position of the SSND. Profiles are calculated using annuli with equal radial steps ($=15''$). The surface density profiles of embedded clusters can be fitted with $1/r$ profiles (e.g., McCaughrean & Stauffer 1994; Jiang et al. 2003; Muench et al. 2003). They also can be fitted with King profiles (e.g., Horner, Lada, & Lada 1997; Nürnberger & Petr-Gotzens 2002; Teixeira et al. 2004). If we can neglect the tidal radius, King profiles can be written as

$$f(r) = \frac{f_0}{1 + (r/r_c)^2}$$

where f_0 is the central surface density and r_c is the core radius (King 1962). Ideally, the radial profile should become zero at $r \rightarrow \infty$. However, in the observation of the actual clusters, the radial profile does not become zero but a constant at $r \rightarrow \infty$ due to the field stars which contribute as a background offset. Therefore, in order to take the contribution from the field stars into account, we added a constant term as a fitting parameter to fitting functions.

The data of the RCW 36 cluster can be well fitted with King profiles better than with

1/r profiles; a departure from King profiles arising around $r \sim 0.2$ pc is due to the southern SSND peak. King profile fitting yields the central density of $f_0 = 3200$ stars pc^{-2} and the core radius of $r_c = 0.08$ pc. Since the column density of isothermal gas sphere in hydrostatic equilibrium has a radial dependence of r^{-1} (Yun & Clements 1991), the 1/r dependence of the SSND radial profile in the embedded clusters is likely to be a footprint of the density profile of their parental cloud core. On the other hand, King models describe solutions for stellar systems in dynamical equilibrium, such as globular clusters. The secondary peak of the SSND, which causes the departure around $r \sim 0.2$ pc in Fig. 3, might be a relic of the primordial substructure that has not fully merged into main body of the RCW 36 cluster (Scally & Clark 2002). Since King profiles better fits the observed radial profile than 1/r profiles overall except for the secondary peak, the dynamical equilibrium would have been almost, if not completely, established in the RCW 36 cluster.

3.2.3. Determination of the Cluster Properties

In order to obtain the fundamental properties of the RCW 36 cluster, such as the number of the stars and radius, we have to estimate the degree of the field star contamination. The frequency distribution of the star counts per unit cell (used to derive SSND in §3.2.1) can be fitted by the Poisson function with a mean of 2 stars per unit cell. This means that uniform background stars are distributed in the whole observed field. Hereafter, we take this value (2.0 stars/unit cell ~ 190 stars pc^{-2}) as the background. This estimation is reasonable because the background value yielded by King profile fitting in the previous section is in good agreement with it.

We can estimate the number of the RCW 36 cluster members by subtracting background from 823 sources detected at K_S with a photometric error of ≤ 0.1 mag. The total expected background population in the observed field is 474 [= 2.0 \times 4 (stars arcmin^{-2}) \times 7.7 \times 7.7 (area of observed field)]. Then, the total number of the cluster members is estimated to be 349; we note that this estimation is a lower limit down to our limiting magnitude. The radial profile merges with the extended background at $r \sim 0.5$ pc (see Fig. 3). We take this as the cluster radius. Considering the background contamination, the SSND of the central 0.1 pc \times 0.1 pc region of the cluster is approximately 3000 stars pc^{-2} ; this is in good agreement with the central density yielded by King profile fitting in the previous section. This is different from the value of ~ 4800 stars pc^{-2} derived by Massi, et al. (2003), but we confirmed in our data that this inconsistency is due to their unit cell size (20'' \times 20''). In table 1, we show the comparison of the central SSND with other embedded clusters within 1 kpc of the Sun. The central SSDN of the RCW 36 cluster is much higher than most of the young clusters

but lower than the Trapezium cluster.

The theory borrowed from the traditional theory of low-mass stars that stars are formed through gravitational collapse of dense molecular cores can only account for those stars with masses less than $10 M_{\odot}$, because radiation pressure of massive stars can halt the collapse and reverse the infall. Bonnell, Matthew, & Zinnecker (1998) presented result of numerical experiments that the massive ($M \geq 10M_{\odot}$) stars can be formed through coalescence of two or more lower mass stars in the center of rich, dense stellar clusters. The most massive star in the RCW 36 cluster (O8-O9) is located at the cluster center; this might imply that it was formed through this mechanism. Hillenbrand (1995) suggested that there is a correlation of the cluster density with the maximum stellar mass in the cluster (i.e. more centrally condensed clusters have more massive stars). In fact, the most massive stars in R CrA, IC 348, and Mon R2 are less massive than that of the RCW 36 cluster, and Trapezium has a more massive star (see table 1). However, the most massive star of NGC 2024 is approximately the same as that of the RCW 36 cluster. We note that the central SSND of NGC 2024 might have been estimated to be too low, because the observation toward NGC 2024 (Lada et al. 1991) was made with relatively small limiting magnitude ($K \sim 14$ mag) and relatively larger pixel scale ($\sim 1''.3$ pixel $^{-1}$). If we assume a distance of 415 pc and mean extinction of $A_V \sim 10.5$ mag toward NGC 2024 (Haisch, Lada, & Lada 2000), the limiting magnitude corresponds to an extinction-corrected absolute magnitude of $M_{K_{A_V=0}} \sim 4.9$ mag. For an assumed age of 1 Myr, their observation could detect down to $\sim 0.09 M_{\odot}$ (Baraffe et al. 1998). In order to take low-mass members of NGC 2024 into account down to our observation limit [$\sim 0.04 M_{\odot}$ assuming a distance of 700 pc, mean extinction of $A_V \sim 8.1$ mag, and an age of ~ 3 Myr (see below)], we use the slope of Trapezium IMF (Muench et al. 2002). The estimated central SSND of NGC 2024 (~ 1700 stars pc $^{-2}$) is still lower than that of RCW 36. However, the larger pixel scale might affect the estimation of the central SSND more seriously, because the radial profile of the SSND for NGC 2024 decreases in the cluster center (see Fig. 8 of Lada et al. 1991).

3.3. color-color diagram

In Fig. 4, we show the J-H v.s. H-K color-color diagram for the 610 sources identified in three bands (see §2). Their colors are transformed to the CIT system with the color equations² (Y. Nakajima, et al. in preparation). The sources falling into a region of infrared excess (the right of the reddening band) in the color-color diagram are considered to be

²<http://www.z.phys.nagoya-u.ac.jp/~sirius/about/color.e.html>

likely cluster members with optically thick, circumstellar disks. The total of 77/349 (22%) of the cluster members exhibit infrared excesses greater than their photometric errors (we note this excess fraction might be just a lower limit because several cluster members were not detected in three bands). We also estimate the mean extinction toward the RCW 36 cluster to be $A_V \sim 8.1$ mag by de-reddening all sources in Fig. 4 back to this CTTS locus (Meyer, Calvet, & Hillenbrand 1997) along the reddening vector.

3.4. K_S Luminosity Function

In Fig. 5, we show the K_S band luminosity function (hereafter KLF) for the RCW 36 cluster. In order to obtain the KLF for the cluster members (cluster KLF), we must remove background contamination. We use the sources which are included in the regions whose SSND is smaller than the background plus 1σ (off-cluster region) to construct the off-cluster KLF. The off-cluster region is approximately the same as the region $r \geq 0.5$ pc from the cluster center. Thus, most of the sources contained in the off-cluster region are supposed to be background stars (see Fig. 3). The off-cluster KLF is shown with open squares and dashed line in Fig. 5a. By subtracting the (scaled) off-cluster KLF from the KLF which includes both the cluster members and the field stars (raw KLF; shown in Fig. 5a with filled circle and solid line), we can obtain the cluster KLF (Fig. 5b). The cluster KLF has a turnover with a peak at $K_S \sim 14$ mag, and then decreases down to the completeness limit.

4. DISCUSSION

4.1. Age of the RCW 36 cluster

NIR imaging surveys revealed that, in embedded clusters, the fraction of the sources which possess NIR excess decreases with the cluster age (Lada 1999; Haisch, Lada, & Lada 2001b). The NIR fraction derived from JHK imaging is approximately 50 % for the young (≤ 1 Myr) embedded clusters [e.g., $50 \pm 7\%$ in Trapezium (Lada et al. 2000); $58 \pm 7\%$ in NGC 2024 (Haisch, Lada, & Lada 2000)]. The fraction decreases to approximately 20 % for more evolved (~ 2 -3 Myr) embedded clusters [e.g., $21 \pm 5\%$ in IC 348 (Haisch, Lada, & Lada 2001a); $16 \pm 3\%$ in NGC 2316 (Teixeira et al. 2004)]. The NIR excess fraction of the RCW 36 cluster (22 %; see §3.3) implies that the age of the RCW 36 cluster is approximately 2-3 Myr.

A similar age is obtained by comparing the KLFs. The comparison of the KLFs of RCW 36, Trapezium and IC 348 is shown in Fig. 6. The KLFs for Trapezium and IC 348,

by Muench et al. (2003), are corrected to absolute magnitudes. Reddening corrections were performed for each KLF by shifting to brighter magnitude by each mean extinction [$A_v \sim 8.1$ mag in RCW 36 (see §3.3), $A_v \sim 2.4$ mag in Trapezium (Prosser et al. 1994), $A_v \sim 4.5$ mag in IC 348 (Lada & Lada 1995)]. Trapezium KLF and RCW 36 KLF are scaled to contain the same number of stars as IC 348. The shape of the KLF of RCW 36 is similar to that of Trapezium, but is shifted toward the fainter magnitude. On the other hand, the KLFs of IC 348 and RCW 36 show good agreement in shape and they have the same broad peak at similar absolute magnitudes.

Muench et al. (2000) presented the result of numerical experiments that the KLFs for young clusters which have the same underlying IMF evolve in a systematic manner with increasing age; they evolve to fainter magnitudes. The IC 348 IMF is nearly identical to the Trapezium IMF (Muench et al. 2003), and they are similar to that derived for other embedded clusters, open clusters, and field stars (e.g., Lada & Lada 2003, and the references therein). Hence, if we assume a universal IMF for the RCW 36 cluster, we infer that the RCW 36 cluster has approximately the same age as IC348, about 2-3 Myr, but is older than Trapezium.

4.2. Mass Segregation

In order to examine the mass segregation in the RCW 36 cluster, we show the stellar distribution by splitting the 823 sources detected at K_S with a photometric error of ≤ 0.1 mag into three magnitude bins ($K_s < 12.0$, $12.0 \leq K_s < 14.0$, and $14.0 \leq K_S$) in Fig. 7. The sources of $K_s < 12.0$ show high central condensation (Fig. 7a). The sources of $12.0 \leq K_S < 14.0$ also show central condensation but are less condensed than the sources of $K_S < 12.0$ (Fig. 7b). The sources of $14.0 \leq K_S$ show no central condensation (Fig. 7c); most of these sources are likely to be background stars because their distribution is uniform. These figures clearly demonstrate an excess of the brighter stars in the cluster center. This is more evident in Fig. 8, which shows the SSND radial profiles for three magnitude bins (the same as above). The central position of each radial profiles are the same as Fig. 3. King profile fitting for each magnitude bins yields the core radii of $r_c = 0.02$ pc (Fig. 8a), 0.13 pc (Fig. 8b), and 0.24 pc (Fig. 8c, was not fitted well because the surface density decreases in the central annulus).

In young embedded clusters, because most members are considered to be in the pre-main sequence (PMS) phase, this tendency could have two possibilities. One is that the sources located in the cluster center are young, and the other is that they are massive. The NIR excess of the PMS stars is caused by optically thick circumstellar disks/envelopes. Since

the circumstellar disks/envelopes become optically thinner with age, the PMS stars which possess NIR excess are considered to be younger than those with no NIR excess. Therefore, if younger stars concentrate in the cluster center, the distribution of the sources which possess NIR excess should be similar to those of the brighter sources. However, as shown in Fig. 8d, the radial profile for the sources which possess NIR excess does not show significant central condensation. Their King profile fitting yields the core radius of $r_c = 0.20$ pc which is clearly larger than that of the sources of $K_s < 12.0$. Therefore, the brightness of the sources in the central region of the RCW 36 cluster is not due to their youth, but due to their massiveness.

Mass segregation can be caused 1) by dynamical evolution and equipartition of energy after star formation and 2) by the process of star formation itself. If mass segregation is caused by dynamical evolution, it occurs in approximately the relaxation time, τ_{relax} , of the cluster (Bonnell & Davies 1998). The relaxation time is roughly

$$\tau_{relax} \sim \frac{0.1N}{\ln N} \tau_{cross}$$

where N is the number of stars contained in the cluster and τ_{cross} is the crossing time (Binney & Tremaine 1987). The crossing time, τ_{cross} , is the time it takes a star to cross the cluster ($\tau_{cross} \sim 2R/v_{disp}$, where R is the radius and v_{disp} is the velocity dispersion of the cluster). In the case of most open clusters, mass segregation is likely caused by dynamical evolution [e.g., Pleiades (Pinfield, Jameson, & Hodgkin 1998)]. However, mass segregation in rich and young embedded clusters, such as the Trapezium cluster, is not considered to be caused by dynamical evolution because they are too young to have dynamically evolved. Here, we estimate the relaxation time for several embedded clusters in table 2. Since the Trapezium cluster has a small age and a large number of stars, the relaxation time is significantly larger than its age in spite of the small crossing time. In other embedded clusters whose SSND is lower, dynamical evolution is generally very unlikely because the cluster sizes are larger, the ages are smaller, or both. However, the relaxation time of the RCW 36 cluster is estimated to be $\sim 2.6 \times 10^6$ yr; this is comparable to the cluster age estimated above. Thus, at least from our data, there is a possibility that the mass segregation in the RCW 36 cluster was caused by dynamical evolution, because the RCW 36 cluster has smaller radius, moderate number of stars, and moderate age. However, this does not rule out the possibility of primordial mass segregation in the RCW 36 cluster because the clusters which dynamical equilibrium are established lost all traces of their initial conditions.

5. CONCLUSION

We have presented deep J, H, K_S observations of the RCW 36 cluster which lies in a $C^{18}O$ clump in the cloud C of the Vela Molecular Ridge. The main conclusions are as follows.

1: The RCW 36 cluster has at least ~ 350 members and a cluster radius of ~ 0.5 pc, and the radial profile of the stellar surface number density can be well fitted with King profiles better than with $1/r$ profiles. In the central $0.1 \text{ pc} \times 0.1 \text{ pc}$ region of the RCW 36 cluster, the stellar surface number density is approximately $3000 \text{ stars pc}^{-2}$. This is much higher than most of the young clusters within 1 kpc of the Sun.

2: We measured the NIR excess fraction of the RCW 36 cluster to be 22 %, compared with those of other embedded clusters, and estimated the age of the RCW 36 cluster is approximately 2-3 Myr. The comparison of background corrected KLF of the RCW 36 cluster with Trapezium and IC 348 also supports this estimation.

3: The RCW 36 cluster shows an excess of the brighter stars in its central region. From the comparison of the radial profiles with the sources of $K_S < 12.0$ mag and the sources with NIR excess, we conclude that this tendency means that more massive stars are located near the cluster center.

It is a pleasure to thank the staff of the South African Astronomical Observatory for their kind support during the observations. We also would like to express our thanks to the anonymous referee for comments and suggestions, which greatly improved the scientific content of the paper. This work is partly supported by Grant-in-Aid for Scientific Research of the Ministry of Education, Culture, Sports, Science, and Technology of Japan.

REFERENCES

- Bachiller, R., Guilloteau, S., & Kahane, C. 1987, *A&A*, 173, 324
- Baraffe, I., Chabrier, G, Allard, F., & Hauschildt, P. H. 1998, *A&A*, 337, 403
- Bik, A., Lenorzer, A., Kaper, L., Comerón, F., Waters, L. B. F. M., Koter, A., & Hanson, M. M. 2003, *A&A*, 404, 249
- Binney, J., & Tremaine, S. 1987, *Galactic Dynamics*. Princeton, NJ: Princeton Univ. Press
- Bonnell, I. A., & Davies, M. B. 1998 *MNRAS*, 295, 691
- Bonnell, I. A., Matthew, R. B., & Zinnecker, H. 1998, *MNRAS*, 298, 93
- Braz, M. A., & Epchtein, N. 1982, *A&A*, 111, 91
- Carpenter, J. M., Snell, R. L., Schloerb, F. P., & Skrutskie, M. F. 1993, *ApJ*, 407, 657
- Carpenter, J. M., Meyer, M. R., Dougrados, C., Strom, S. E., & Hillenbrand, L. A. 1997, *AJ*, 114, 198
- Haisch, K. E., Lada, E. A., & Lada, C. J. 2000, *AJ*, 120, 1396
- Haisch, K. E., Lada, E. A., & Lada, C. J. 2001a, *AJ*, 121, 2065
- Haisch, K. E., Lada, E. A., & Lada, C. J. 2001b, *ApJ*, 553, L153
- Hillenbrand, L. A. 1995 Ph.D. Thesis University of Massachusetts
- Hillenbrand, L. A., & Hartmann, L. W. 1998, *ApJ*, 492, 540
- Hodapp, K. W., 1994, *ApJS*, 94, 615
- Horner, D. J., Lada, E. A., & Lada, C. L., 1997, *AJ*, 113, 1788
- Jiang, Z., et al. 2003, *ApJ*, 596, 1064
- Jones, B. F., & Walker, M. F. 1988, *AJ*, 95, 1755
- King, I., 1962, *AJ*, 67, 471
- Koornneef, J. 1983, *A&A*, 128, 84
- Lada, C. J., Muench, A. A., Haisch, K. E., Lada, E. A., Alves, J. F., Tollestrup, E. V., & Willner, S. P. 2000, *AJ*, 120, 3162

- Lada, C. J., & Lada, E. A. 2003, *ARA&A*, 41, 57
- Lada, E. A., Depoy, D. L., Evans, J. H., & Gatley, I. 1991, *ApJ*, 371, 171
- Lada, E. A., & Lada, C. J. 1995, *AJ*, 109, 1682
- Lada, E. A. 1999, *The Origin of Stars and Planetary Systems*, edited by Lada, C. J., & Kylafis, N. D. (Kluwer Academic Publishers), p. 441
- Liseu, R., Lorenzetti, D., Nisini, B., Spinoglio, L., & Moneti, A. 1992, *A&A*, 265, 577
- Lorenzetti, D., Spinoglio, L., & Liseu, R. 1993, *A&A*, 275, 489
- Massi, F., Lorenzetti, D., & Giannini, T. 2003, *A&A*, 399, 147
- McCaughrean, M. J., & Stauffer, J. R. 1994 *AJ*, 108, 1382
- Meyer, M. R., Calvet, N., & Hillenbrand, L. A. 1997, *ApJ*, 114, 288
- Miesch, M.S., & Bally, J. 1994, *ApJ*, 429, 645
- Muench, A. A., Lada, E. A., & Lada, C. J. 2000 *ApJ*, 533, 358
- Muench, A. A., Lada, E. A., Lada, C. J., & Alves, J. 2002 *ApJ*, 573, 366
- Muench, A. A., et al. 2003, *AJ*, 125, 2029
- Murphy, D. C., & May, J. 1991, *A&A*, 247, 202
- Nagashima, C., et al. 1999, in *Star Formation 1999*, ed. T. Nakamoto (Nobeyama: Nobeyama Radio Obs.), p. 397
- Nagayama, T., et al. 2002, *Proc. SPIE*, 4841, 51
- Nürnberg, D. E. A., & Petr-Gotzens, M. G. 2002, *A&A*, 382, 537
- Persson, S. E., Murphy, D. C., Krzeminski, W., Roth, M., & Rieke, M. J. 1998, *AJ*, 116, 2475
- Pinfield, D. J., Jameson, R. F., & Hodgkin, S. T. 1998, *MNRAS*, 299, 955
- Prosser, F. P., Stauffer, J. R., Hartmann, L., Soderblom, D. R., Jones, B. F., Werner, M. W., & McCaughrean, M. J. 1994, *ApJ*, 421, 517
- Scally, A., & Clarke, C. 2002, *MNRAS*, 334, 156

- Teixeira, P. S., Fernandes, S. R., Alves, J. F., Correia, J. C., Santos, F. D., Lada, E. A., & Lada, C. J. 2004, *A&A*, 413, L1
- Tokunaga, A. T. 1996, *Astrophysical Quantities*, 4th edition, ed. Cox, A. (AIP Press), p. 143
- Verma, R. P., Bisht, R. S., Ghosh, S. K., Iyenger, K. V. K., Rengarajan, T. N., & Tandon, S. N. 1994, *A&A*, 284, 936
- Walsh, A. J., Burton, M. G., Hyland, A. R., & Robinson, G. 1998, *MNRAS*, 301, 640
- Wilking, B. A., McCaughrean, M. J., Murton, M. G., Giblin, T., Rayner, J. T., & Zinnecker, H. 1997, *AJ*, 114, 2029
- Yamaguchi, N., Mizuno, N., Saito, H., Matsunaga, K., Mizuno, A., Ogawa, H., & Fukui, Y. 1999, *PASJ*, 51, 775
- Yun, J. L., & Clemens, D. P. 1991, *ApJ*, 381, 474
- Zinnecker, H., McCaughrean, M. J., & Wilking, B. A. 1993 in *Protostars and Planets III*, ed. Levy, E. H., & Lunine, J. I. (The Univ. of Arizona Press), p. 429

Fig. 1.— JHK_S three-color composite image of the RCW 36 cluster. (J : *blue*, H : *green*, K_S : *red*) obtained with IRSF/SIRIUS. North is up, and east is to the left. The plus represents the peak position of radio continuum (Walsh et al. 1998), and the asterisk represents the position of H₂O maser (Braz & Epchtein 1982). [Figure separately included as gif (to make smaller).]

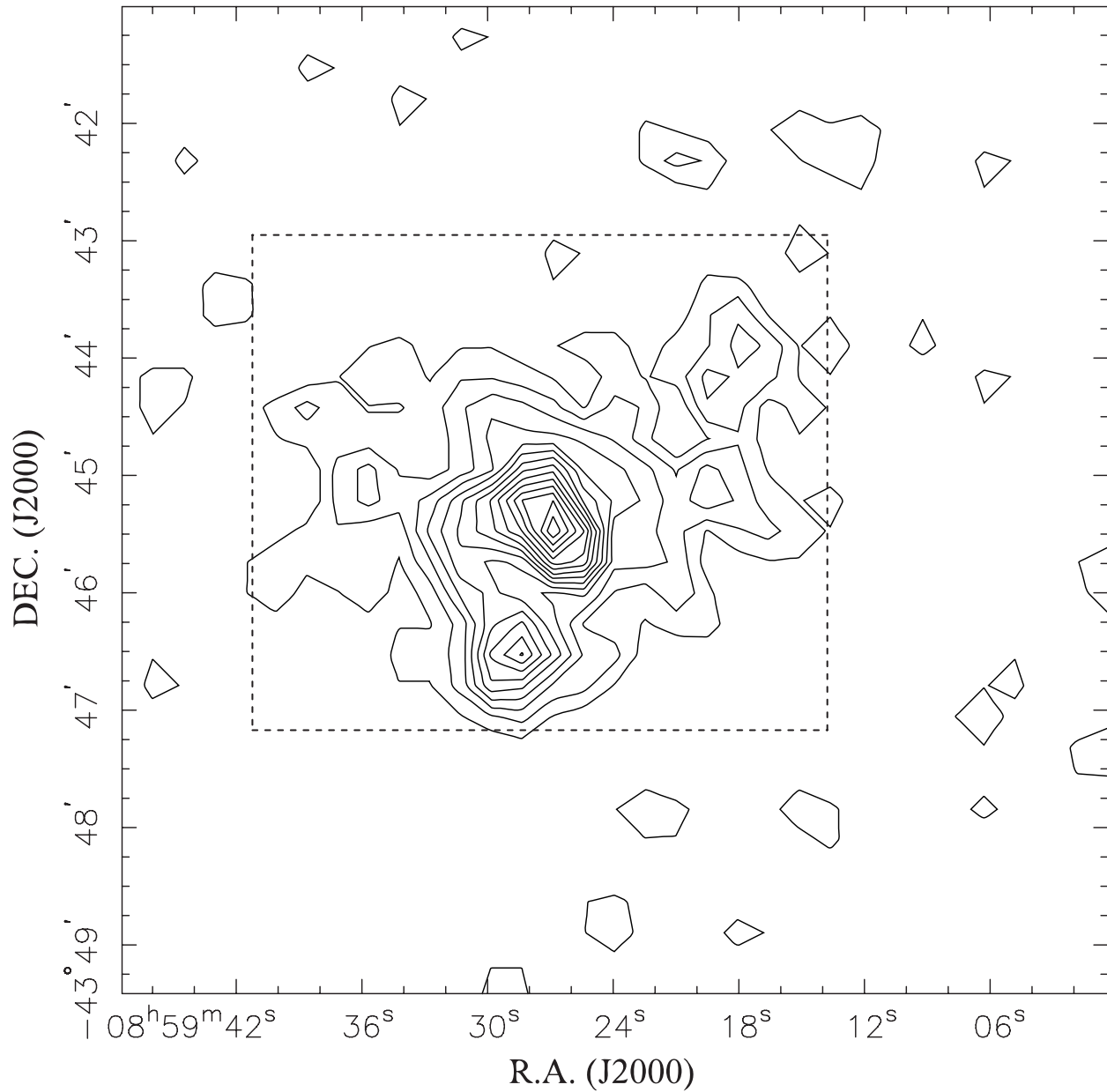


Fig. 2.— Contour map of the stellar surface number density obtained by counting stars in a $30'' \times 30''$ ($\sim 0.1 \text{ pc} \times 0.1 \text{ pc}$ at 700 pc) area every $15''$ over the K_S image. The lowest contour is $400 \text{ stars pc}^{-2}$, and steps are $200 \text{ stars pc}^{-2}$. Dotted square is the region used to determine the completeness limits (see §2).

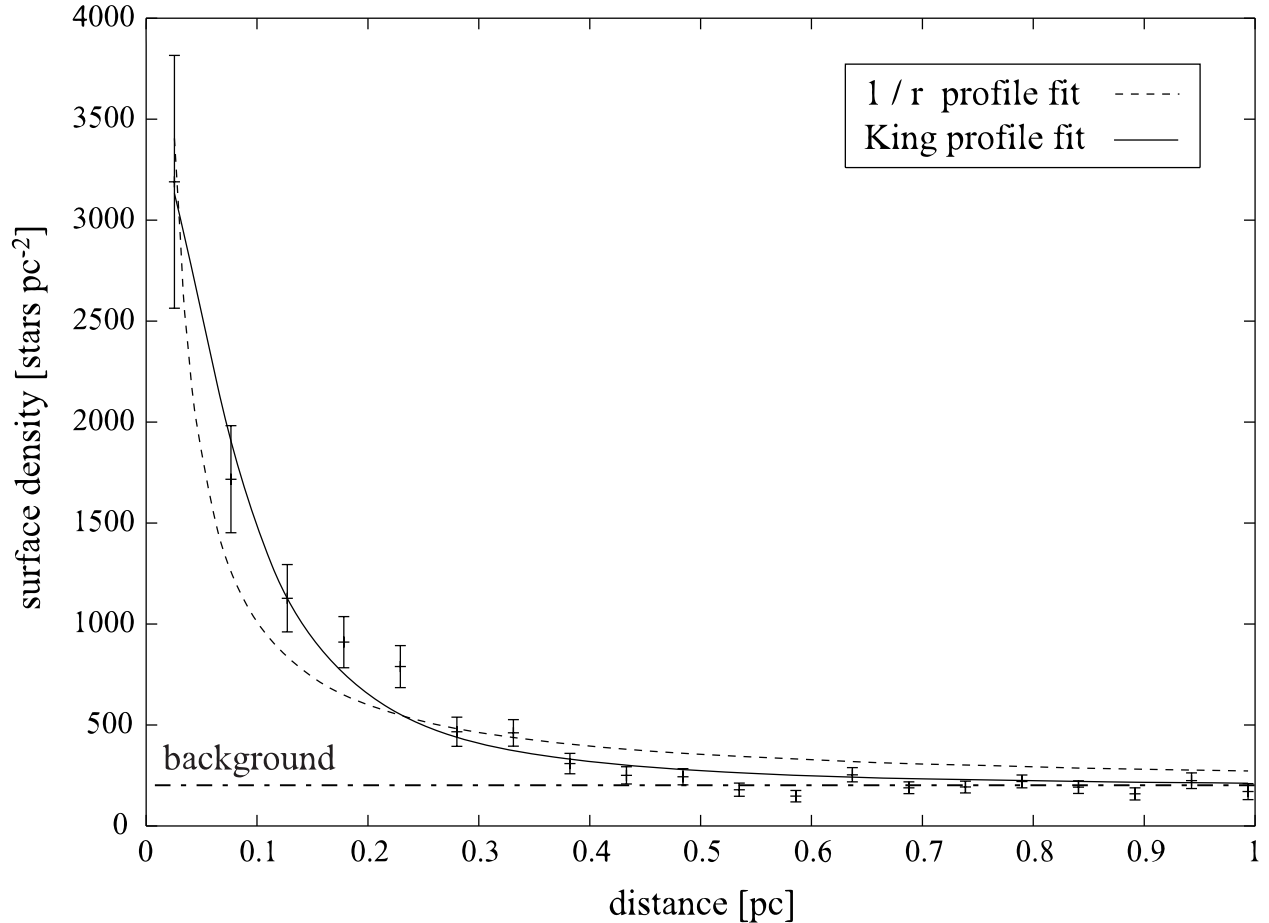


Fig. 3.— Radial profile of the stellar surface number density for the RCW 36 cluster. Stellar surface density (in stars per pc²) is measured in circular annuli, centering on the location of the peak position of the stellar surface density (see Fig. 2). Profiles are calculated using annuli with equal radial steps (=15"). The errors are statistical \sqrt{N} error. The horizontal dot-dashed line corresponds to background surface density [level = 2.0 stars in a 30" \times 30" unit cell (see §3.2.3)]. The solid curve represents a King profile fit, and the dashed curve represents a 1/r profile fit.

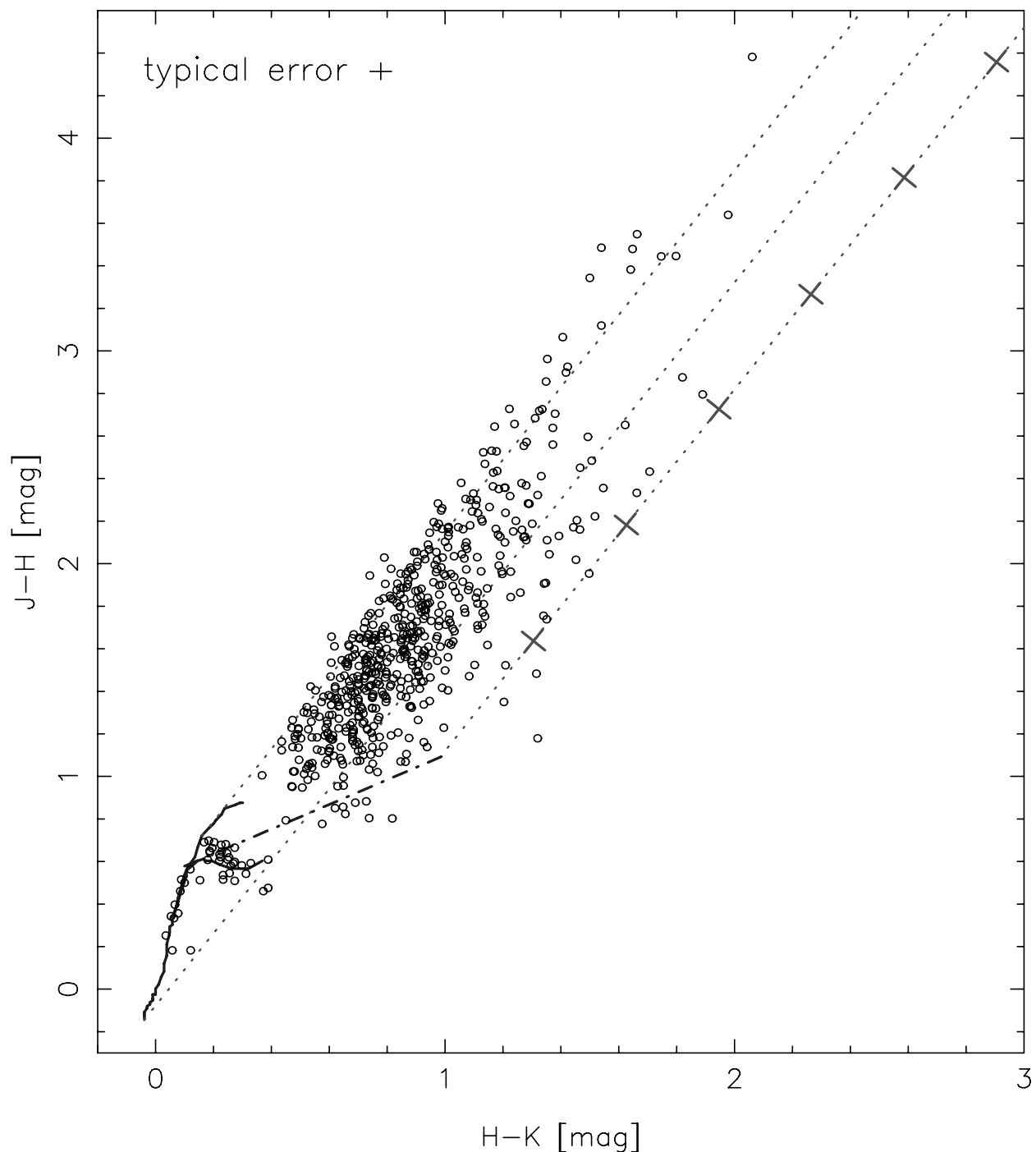


Fig. 4.— The color-color diagram for the sources in the RCW 36 cluster with J , H , K_S band photometric errors ≤ 0.1 mag. The solid lines represent the loci of dwarfs and giants (Tokunaga 1996), the dot-dashed line represents the locus of unreddened Classical T Tauri Stars (CTTS) (Meyer, Calvet, & Hillenbrand 1997). The two leftmost parallel dashed lines define the reddening band for dwarfs and giants. They are parallel to the reddening vector. The tick marks on the reddening line indicate 5 mag intervals in A_v from the right edge of the CTTS locus. The reddening law of Koornneef (1983), having the slope of 1.7, is adopted.

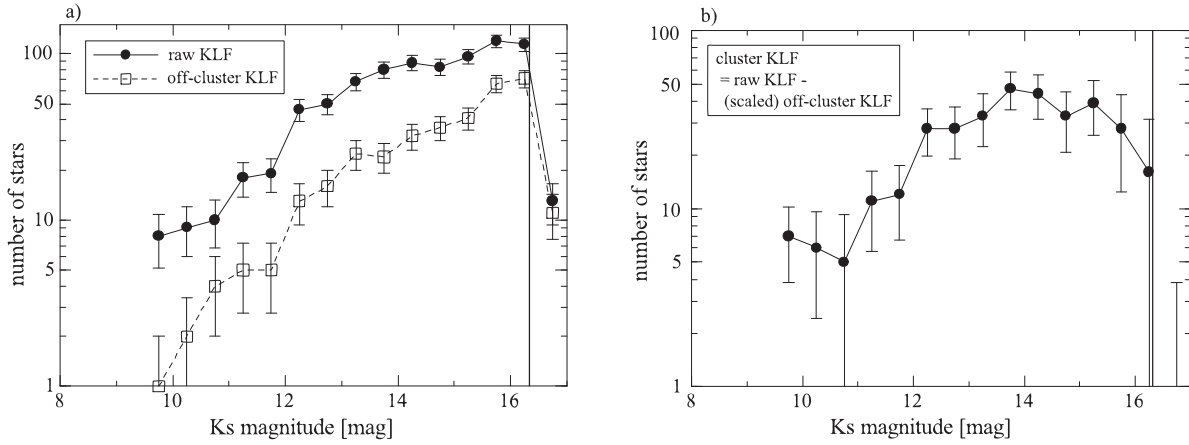


Fig. 5.— The KLFs of the RCW 36 cluster. The bin width is 0.5 mag, and the errors are statistical \sqrt{N} error. The solid vertical line represents 90 % completeness limit. a): The filled circles with solid line are “raw KLF” (from all sources detected in the K_S band with a photometric error of ≤ 0.1 mag), and the open squares with dashed line are the “off-cluster KLF” [from the sources detected in the K_S band with a photometric error of ≤ 0.1 mag and are located in the off-cluster region (the region whose SSNDs are \leq background + 1σ)]. b): The KLF for the RCW 36 cluster members. In order to obtain this KLF, the off-cluster KLF (scaled to account for the different areas) is subtracted from the raw KLF.

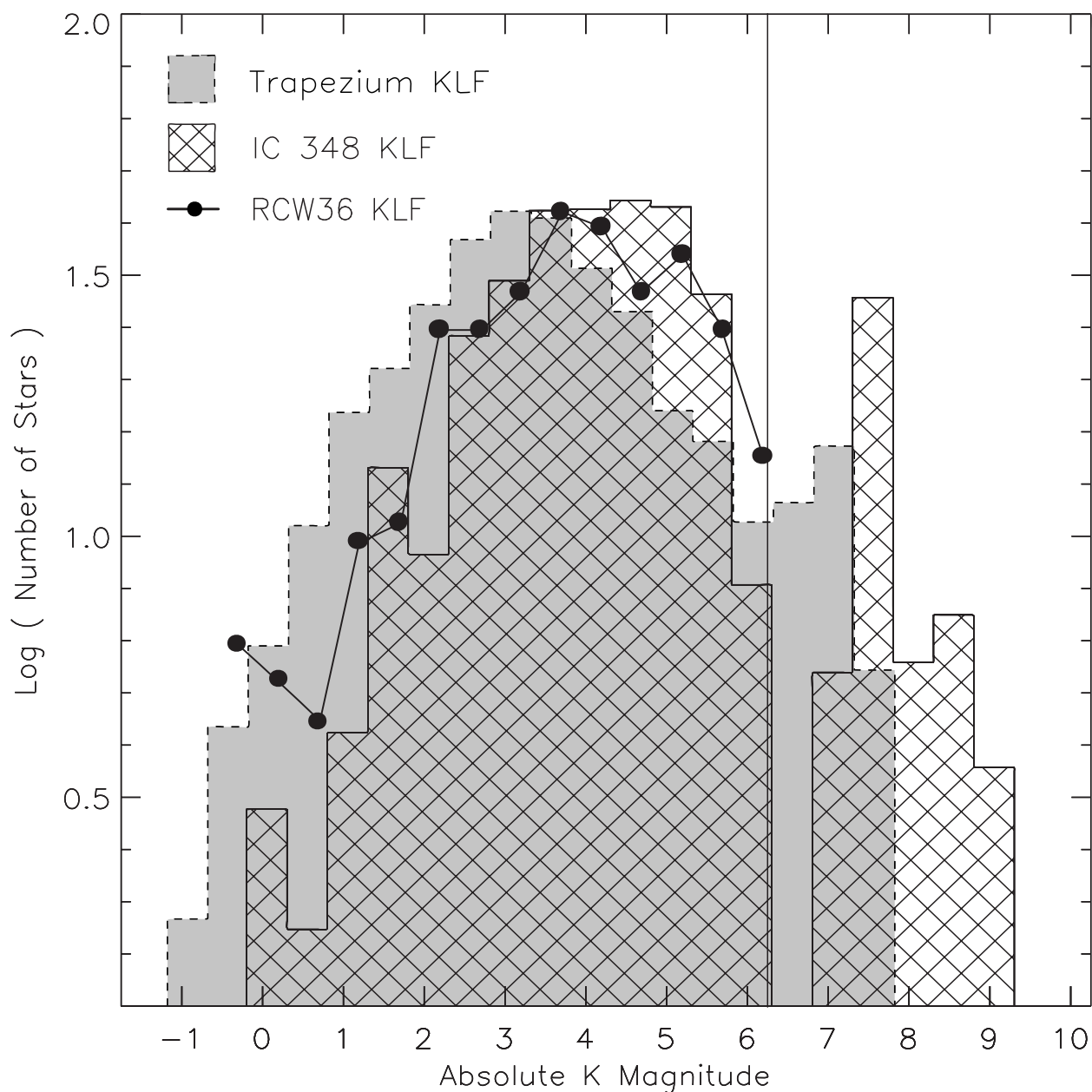


Fig. 6.— The comparisons of the background subtracted KLFs. All magnitudes are shifted to absolute magnitudes. The Trapezium and RCW 36 KLFs have been scaled to contain the same number of stars as IC 348. The KLFs for IC348 and Trapezium are obtained by Muench et al. (2003). The solid vertical line represents our 90 % completeness limit. Reddening correction was performed by shifting each KLF toward the brighter magnitude by each mean extinction (see §4.1).

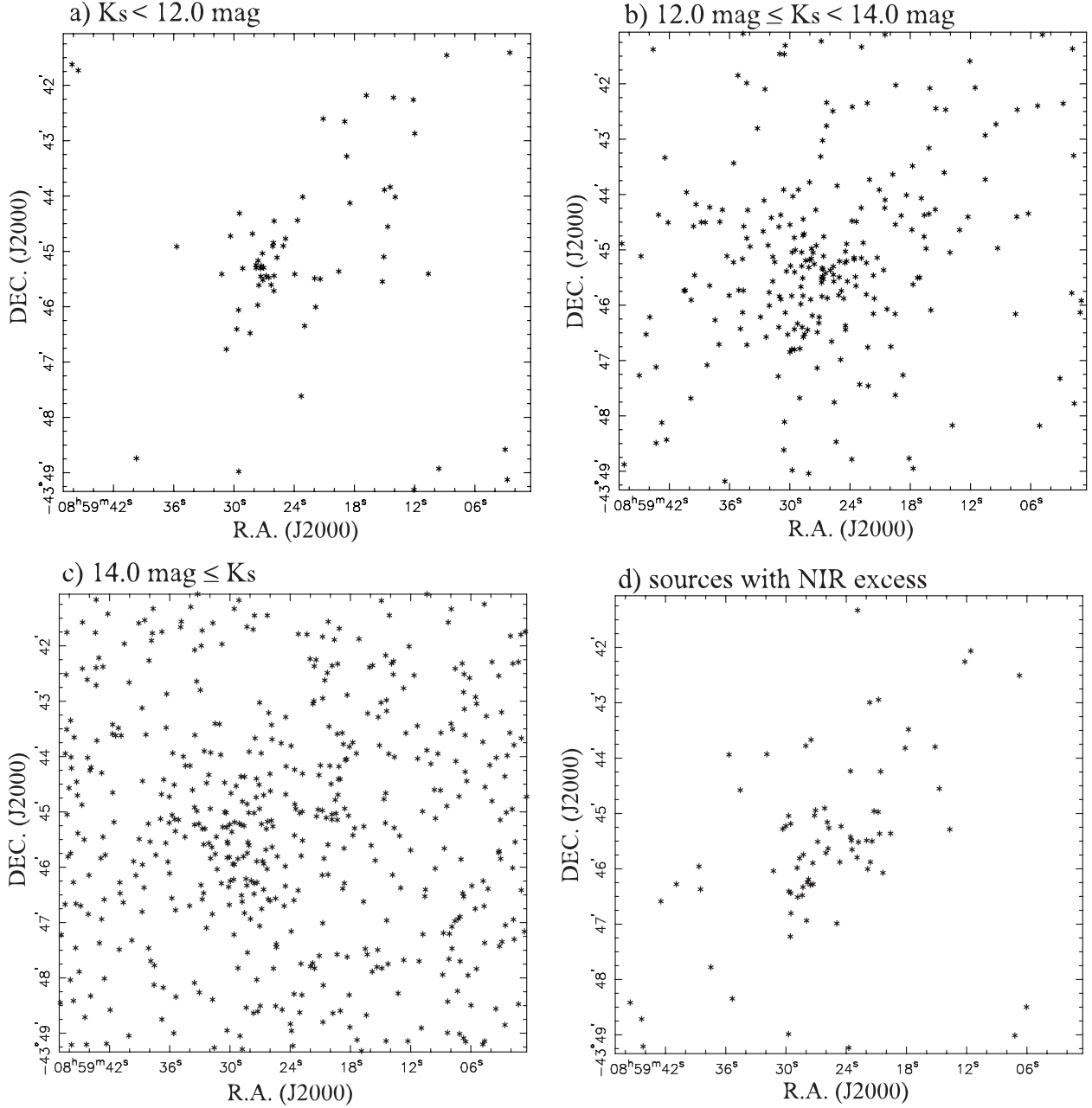


Fig. 7.— a) - c): The distributions of the sources detected in the K_S band with a photometric error of ≤ 0.1 mag [a): the sources of $K_S < 12.0$, b): the sources of $12.0 \leq K_S < 14.0$, c): the sources of $14.0 \leq K_S$]. d): The distributions of the sources identified in three bands and falling into a region of infrared excess in Fig. 4.

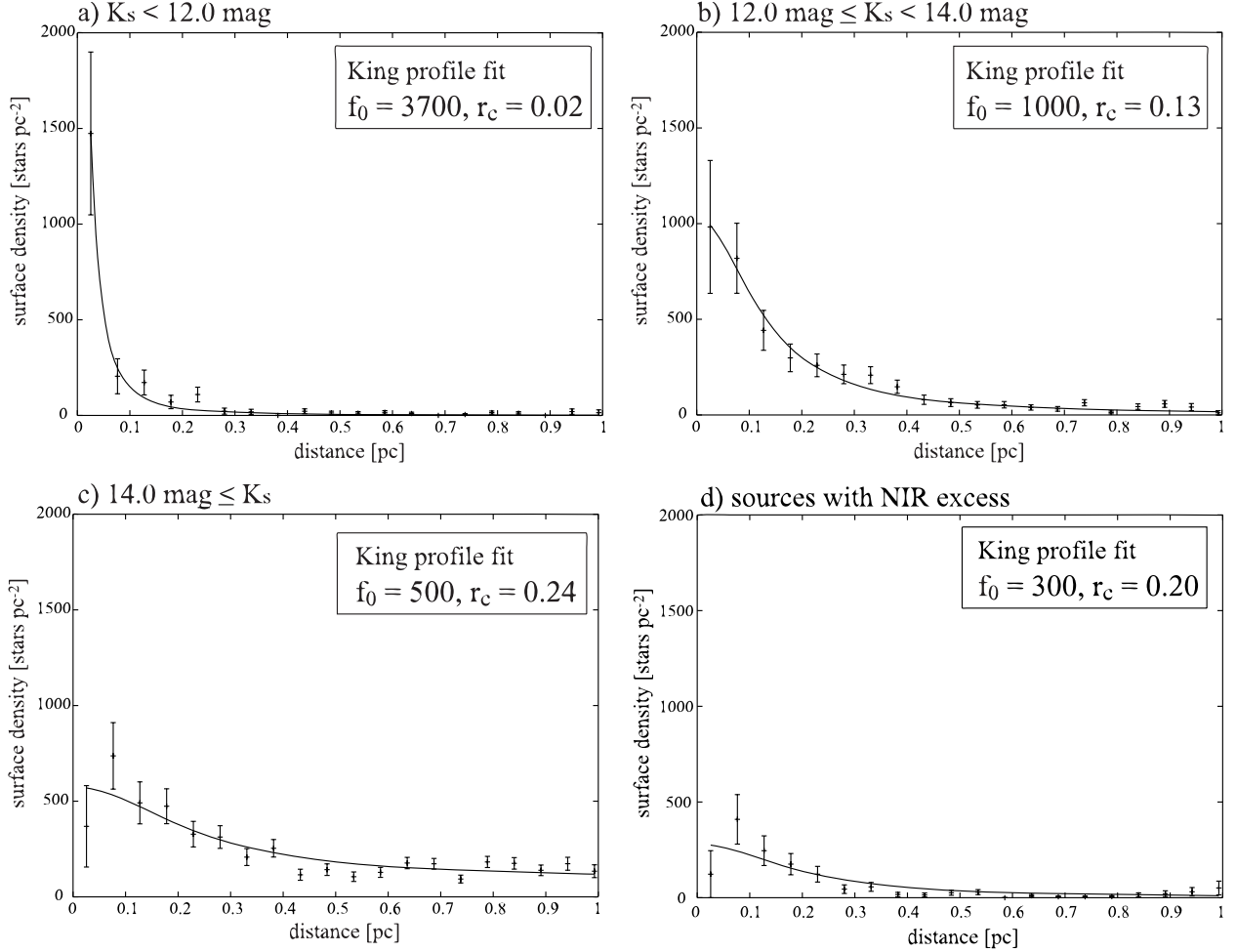


Fig. 8.— Radial profiles of the stellar surface number density for the RCW 36 cluster. The errors are statistical \sqrt{N} error. a): the sources of $K_S < 12.0$, b): the sources of $12.0 \leq K_S < 14.0$, c): the sources of $14.0 \leq K_S$, d) the sources with NIR excess (see §3.3). The photometric errors for all sources are ≤ 0.1 mag. The solid lines represent King profile fits.

Table 1. Comparison of the most massive star and the central SSND

Region	Distance [pc]	Most massive [Sp type]	Central SSND [stars pc ⁻²]	K (limit)	References
R CrA	150	B9	260 ^a	16.5	1
IC348	320	B5	955 ^a	15.0	2
NGC2024	415	O8	1600 ^a	14.0	3, 4, 5
MonR2	830	B0	1900 ^c	14.5	6
Trapezium	470	O7	5600 ^b	17.0	7
RCW 36	700	O8-O9	3000 ^a	16.3	this work

^ainner central 0.1 pc

^byielded by King profile fit

^cyielded by Gaussian profile fit

References. — (1) Wilking et al. (1997); (2) Lada & Lada (1995); (3) Lada et al. (1991); (4) Bik et al. (2003); (5) Haisch, Lada, & Lada (2000); (6) Carpenter et al. (1997); (7) Hillenbrand & Hartmann (1998)

Table 2. Estimation of the Relaxation time

Region	Size [pc]	N_{star}	v_{disp} [km s ⁻¹]	τ_{cross} [Myr]	τ_{relax} [Myr]	Cluster Age [Myr]	References
IC348	1.0	300	1.0 ^a	2.0	10	2-3	1, 2, 3
NGC2024	0.88	309	1.3 ^b	1.3	7.1	1	1, 4, 5
MonR2	1.85	371	1.1 ^b	3.3	21	<3	1, 4, 6
Trapezium	0.24	780	2.5 ^c	0.13	2.2	<1	1, 7, 8
RCW 36	0.5	349	2.2 ^a	0.44	2.6	2-3	this work, 9

^a Δv of C¹⁸O

^b Δv of ¹³CO

^cvelocity dispersion of the stars

References. — (1) Lada & Lada (2003) and references therein; (2) Bachiller, Guilloteau, & Kahane (1987); (3) Haisch, Lada, & Lada (2001a); (4) Miesch & Bally (1994); (5) Haisch, Lada, & Lada (2000); (6) Carpenter et al. (1997); (7) Jones & Walker (1988); (8) Hillenbrand & Hartmann (1998); (9) Yamaguchi et al. (1999)

This figure "f1.gif" is available in "gif" format from:

<http://arxiv.org/ps/astro-ph/0406645v1>